AQUA
Water Infrastructure, Ecosystems and Society

IWA PUBLISHING

 AQUA — Water Infrastructure, Ecosystems and Society Vol 73 No 3, 487 doi: 10.2166/aqua.2024.260

Exploring the air impacts on the state development of pipe flow using the smooth particle hydrodynamic method

Zixuan Zheng[a], Xinwei Cai[b], Feifei Zheng[a], Xin Bian[b,*], Hongwu Tang[c], Saiyu Yuan[c] and Yiyi Ma[a]

[a] College of Civil Engineering and Architecture, Zhejiang University, Hangzhou 310058, China
[b] State Key Laboratory of Fluid Power and Mechatronic Systems, Department of Engineering Mechanics, Zhejiang University, Hangzhou 310027, China
[c] Key Laboratory of Hydrologic-Cycle and Hydrodynamic System of Ministry of Water Resources, Hohai University, Nanjing 210098, China
*Corresponding author. E-mail: bianx@zju.edu.cn

XB, 0000-0002-7641-4715

ABSTRACT

It is widely recognized that the water flow in pipes can be affected by trapped air pockets. However, the underlying air–water interactions of free flow with non-jacking downstream of the pipe are rarely investigated. There are no studies at this time that clearly elucidate the differences in pipe flow between the vacuum and the presence of air in the free flow case. To this end, the smoothed particle hydrodynamics (SPH) method is applied to study the air–water hydraulic dynamics in the pipe under free flow. We perform SPH simulations in several different scenarios and find that (i) the SPH method is competent to simulate both single- and two-phase flows in the pipe due to its outstanding advantages in capturing complex interfaces; (ii) only when the upstream water level is higher than the top of the pipe inlet, and the water level in the pipe rises to the top of the pipe due to air resistance, can a full pipe flow be formed; and (iii) the presence of air can cause the water to form a full pipe flow, causing a siphon-like effect that promotes pipe drainage. These results provide insights into the underlying complex air–water hydraulic properties in pipe flows.

Key words: air impacts, pipe flow rate, pipe flow state, smooth particle hydrodynamic method

HIGHLIGHTS

- The smoothed particle hydrodynamics method is performed for air–water simulations of pipe drainage.
- The air–water hydraulic dynamics in the pipe under free flow conditions are systematically explored by analyzing changes in the flow rate and flow state.
- The results show that, contrary to the commonly recognized blocking effect of trapped air in submerged flow, air in free flow can actually facilitate pipe draining.

GRAPHICAL ABSTRACT

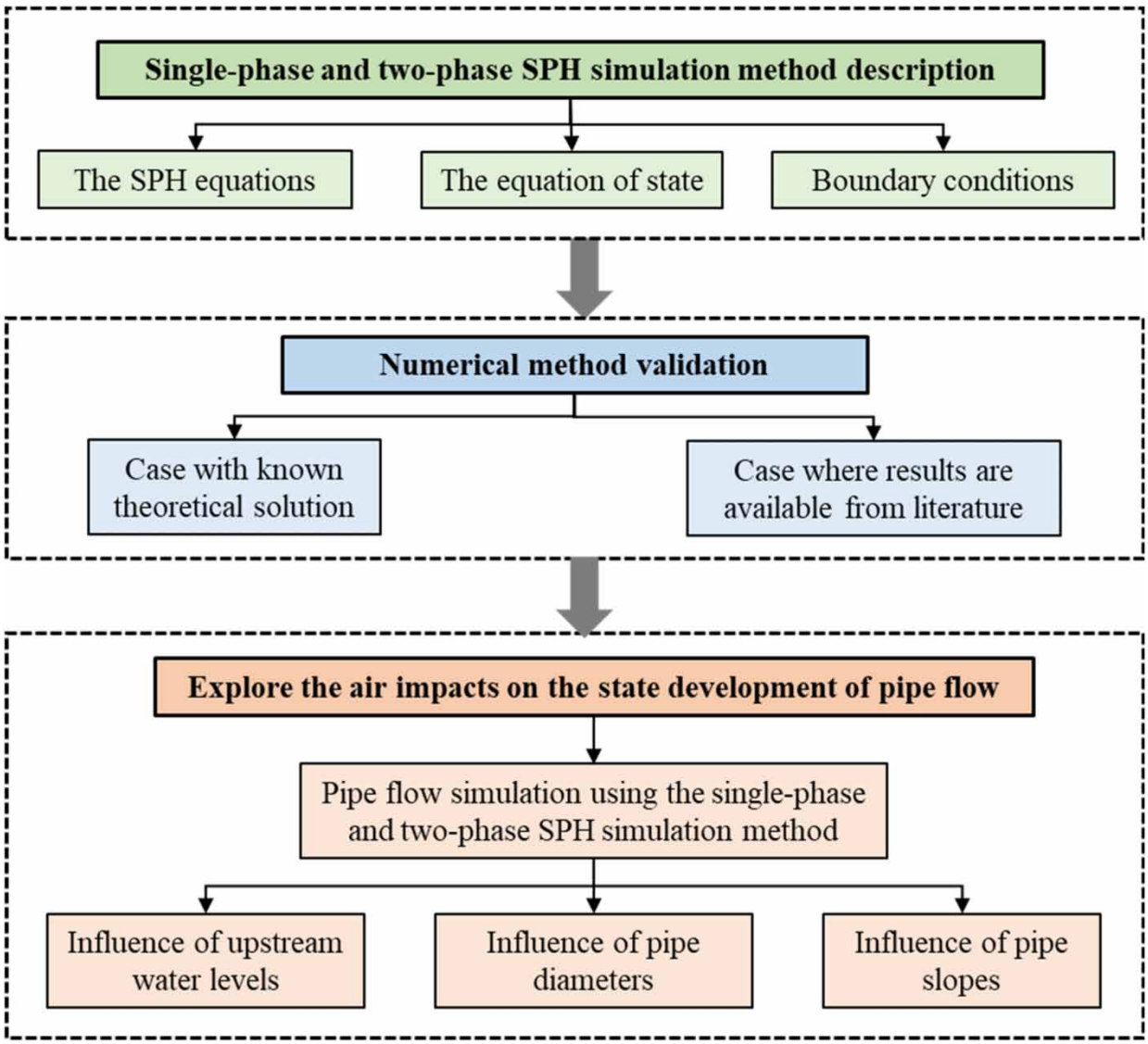

1. INTRODUCTION

Urban flooding has emerged around the world, seriously affecting social and economic development and even threatening the lives of residents (Zheng *et al.* 2015). According to a study by Winsemius *et al.* (2016), urban flooding in the world from 1980 to 2014 has resulted in cumulative direct economic losses of about one trillion dollars and the deaths of about 220,000 people. Recently, the torrential rainstorm that took place in Zhengzhou, China, in 2021, known as the '7.20' event, caused 292 deaths and 120 billion RMB economic losses (ChinaNews 2022). Therefore, the prevention and control of urban flooding has become one of the most important requisites for the sustainable development of cities.

Urban flooding is affected by many factors, and the flow capacity of pipes is one of them. Thus, it is important to understand the drainage mechanism of pipes to prevent urban flooding. With the in-depth study of pipes, more and more researchers have found that considering hydraulic factors alone cannot accurately describe the dynamic process of pipe drainage. This is because the interaction between air and water in the pipes also significantly affect the drainage capacity (Wang *et al.* 2012). More specifically, most drainage pipes drain by gravity, which are non-full or partly full flows, so there are both water and air in the pipe (Qian *et al.* 2021). In addition, the operation of the drainage system also causes air to enter the pipe, such as falling water entrainment, equipment operation inhalation, air decomposition in water, and so on. Due to

the limited space inside the pipe, the air cannot escape quickly and freely and, therefore, coexists with the water inside the pipe (Qian *et al.* 2021). As a result, a series of complex air–water interactions occur in the pipes, which affects the flow capacity. The studies by Zhou *et al.* (2013) pointed out that the presence of air in the pipe impedes the water flow at both ends of the air pocket, changing the flow velocity and direction of the water flow.

To clarify the air–water interaction of pipes, many experiments have been carried out. Current experimental research studies focus mainly on the formation law of air pockets and the analysis of the characteristics of air–water flow. Vasconcelos & Wright (2007) summarized the formation of air pockets into two mechanisms, namely, the jacking action interception and the refraction shock wave interception. Subsequently, Pozos *et al.* (2010) observed that the movement of air pockets in the pipe is affected by the pipe length and diameter, and they are more likely to accumulate in pipes with longer lengths and smaller diameters. As for the research on the characteristics of air–water flow in pipes, hydraulic experiments were first conducted to study the flow of water and air in horizontal and slightly inclined pipes. Later, researchers summarized the flow patterns in the pipe as bubble flow, plug flow, slug flow, stratified smooth flow, stratified flow, and annular flow.

In parallel with the research studies based on experiments, numerical methods have been gradually developed. The latter can avoid the randomness of the former and also capture some details that are infeasible to the former, which is beneficial to the analysis of the underlying mechanism. At present, numerical simulations of air–water flow in pipes generally adopt mesh-based methods, such as those implemented in Fluent and OpenFOAM. For instance, He *et al.* (2022) described the dynamic behavior of an isolated slug driven by pressurized air in a voided line with an end orifice using Fluent. Although these mesh-based methods are mature and widely used, their mesh generation process is tedious and often requires a lot of trials to achieve high-quality meshes. In addition, most of these methods require additional processing (e.g., volume of fluid, level set function) to track interfaces, which makes it formidable to deal efficiently with problems such as free surfaces, deformable boundaries, and moving interfaces (Liu & Liu 2003).

Compared to the mesh-based methods, mesh-free methods typically adopt particles to partition the computational domain and simulate fast and large displacement of flows relatively easily, especially on freely moving surfaces (Liu & Liu 2003). As one of the most mature mesh-free methods, the smoothed particle hydrodynamics (SPH) has attracted wide attention in the field of multi-phase flow (Hu & Adams 2006; Dong *et al.* 2022; Cai *et al.* 2023; Wang *et al.* 2023). Many researchers have performed a series of water–air simulations using SPH, such as water–air wave impact (Lind *et al.* 2015), free floating bubble movement in water (Meister & Rauch 2015; Zhang *et al.* 2015), water ingress considering air effects (Meng *et al.* 2021), and so on. In 2012, Hou *et al.* (2012) first attempted to apply the SPH method to simulate the pipe flow and verified the feasibility of the SPH method in pipe flow simulations. Recently, Song *et al.* (2023) used the SPH method to solve water hammer equations for pipeline systems and compared the simulation results with the data from the experimental tests and classical method of characteristics (MOC) results. However, they used air as the boundary condition and did not really apply SPH to realize the two-phase flow simulation in the pipe.

Although the above studies have made great contributions to the field of water–air pipe flows, there are still some shortcomings. In particular, most of the existing studies inject the mixture of water and air into the pipe or set up an air pocket in the pipe at the initial moment to study the flow patterns. These studies focus on the interaction between entrapped air pockets and water in the pipe, based on scenarios in which air pockets are already trapped in pipes. However, the effect of air on pipe flow in the case of free flows without jacking downstream of the pipes is rarely explored, even though this is the most common drainage scenario in real projects. To the best of our knowledge, there is currently no literature that clearly elucidates the influence of air in the pipe on the pipe flow state development and pipe flow rate change under free flow conditions. Moreover, current research is often only carried out in the presence of air, taking into account the influence of different factors on the formation and development of air pockets as well as the two-phase flow. It is not straightforward for grid-based methods to deal with both single- and two-phase flows in a universal setting. Therefore, these studies are not comprehensive as they did not compare the results to vacuum conditions (i.e., no air), and one cannot directly distinguish whether an effect is due to the presence of air or still occurs in the absence of air.

To address the above research gap and to gain insight into the underlying mechanisms within the air effects, in this study, the SPH method is used to characterize the single-phase flow (i.e., no air) and two-phase flow (i.e., air and water) processes in pipes due to its advantages in modeling multi-phase flow and capturing interfaces. This study analyzes the impact of air in the case of free flow conditions with non-jacking downstream of the pipes. Specifically, in the case of free outflow conditions, as drainage proceeds, the water level in the upstream manhole decreases and that in the downstream one increases from zero.

Through a series of simulations, the pipe flow patterns and flow capacity changes in vacuum and in the presence of air are compared, and the impacts of air on the pipe flow are clarified.

This paper is organized as follows. The numerical method is described in Section 2. This is followed by the validation of the method in Section 3. Thereafter, the application of the validated method to pipe flows is presented in Section 4. Finally, the main findings and implications of this study are summarized in Section 5.

2. METHODOLOGY

2.1. The SPH equations

In SPH, the value of a function f at particle i is approximated by the average of those values of the function at each surrounding particle j ($j = 1, 2, ..., N$, where N is the total number of particles in the support domain of i) weighted by a kernel function. Therefore, the Navier–Stokes equations in a Lagrangian frame can be expressed in the form of ordinary differential equations (ODEs). In this study, a quintic spline kernel with a cutoff radius $r_c = 3h$ is used as the kernel function, and the smoothing length h of the function is the uniform distance Δx of the initial particle arrangement.

2.1.1. Continuity equation

The discretized form of the continuity for particle i is

$$\frac{d\rho_i}{dt} = \rho_i \sum_j^N \frac{m_j}{\rho_j} \mathbf{v}_{ij} \cdot \nabla_i W_{ij} \tag{1}$$

where t, m, and ρ denote the time, the mass, and the density, respectively; $\mathbf{v}_{ij} = \mathbf{v}_i - \mathbf{v}_j$ is the relative velocity of particles i and j; $\nabla_i W_{ij}$ is the gradient of the smoothing function. Note that this form of density solution is available for multi-phase flow problems because it only considers volume contributions m/ρ, not mass or density alone. However, by using Equation (1), the consistency between mass, density, and occupied area cannot be enforced exactly. To overcome this problem, the density field should be re-initialized periodically. In this study, we used the summation density approach to realize density re-initialization.

2.1.2. Momentum equation

According to Hu & Adams (2006), the momentum equation of particle i can be written as Equation (2). The acceleration of particle i is caused by three parts of forces, namely, pressure gradient, shear forces, and body forces, which are expressed as the first, second, and third terms on the right-hand side of Equation (2).

$$\frac{\mathrm{d}\mathbf{v}_i}{\mathrm{d}t} = -\frac{1}{m_i} \sum_j^N \left(\frac{p_i}{\sigma_i^2} + \frac{p_j}{\sigma_j^2} \right) \nabla_i W_{ij} + \sum_j^N m_j \Pi_{ij} \nabla_i W_{ij} + \mathbf{g} \tag{2}$$

where p and $\mathbf{g}$ denote the pressure and body force, respectively; σ is a measure of the particle number density, with values greater in dense particle regions than that in sparse particle regions (Hu & Adams 2006). Replacing particle density ρ with number density σ avoids numerical instability caused by density discontinuities along interfaces in multi-phase flow scenarios with density ratios (e.g., water and air). Π_{ij} is an artificial viscosity added to the momentum equation to reduce possible oscillations, which has the general form as in Monaghan (1994).

$$\Pi_{ij} = \alpha h_{ij} c_{ij} \frac{(\mathbf{v}_i - \mathbf{v}_j) \cdot (\mathbf{r}_i - \mathbf{r}_j)}{\rho_{ij} (|\mathbf{r}_i - \mathbf{r}_j|^2 + 0.01 h_{ij}^2)} \tag{3}$$

where the coefficients $h_{ij} = 1/2(h_i + h_j)$, $c_{ij} = 1/2(c_i + c_j)$, and $\rho_{ij} = 1/2(\rho_i + \rho_j)$ are the averages of the smoothing length, the sound speed, and the density of particle i and particle j, respectively. α is the artificial viscosity parameter, and its equivalent effective physical kinematic viscosity ν can be calculated by

$$\nu = \frac{1}{2(d+2)} \alpha h_{ij} c_{ij} \tag{4}$$

where d is the number of simulation dimensions. Note that the research objects of this study are all inviscid fluids. To ensure the stability of the flow field, the artificial viscosity parameter α between two phases is set to be non-zero.

2.2. The equation of state

For the simulation of incompressible flows, the weakly compressible formulation of SPH is used, where the pressure p and the density ρ is related through an equation of state. The equation of state reads as follows:

$$p_w = p_0\left[\left(\frac{\rho_w}{\rho_0^w}\right)^{\gamma_w} - 1\right] + \chi \tag{5}$$

$$p_a = p_0\left[\left(\frac{\rho_a}{\rho_0^a}\right)^{\gamma_a} - 1\right] + \chi \tag{6}$$

where the symbols w and a represent water and air, respectively; ρ_0 is the reference density; and χ is the background pressure of the initial pressure field. For the air–water interface, typical adopted values are $\gamma_w = 7$ and $\gamma_a = 1.4$, respectively. The reference pressure p_0 can be described as

$$p_0 = \frac{c_w^2 \rho_0^w}{\gamma_w} = \frac{c_a^2 \rho_0^a}{\gamma_a} \tag{7}$$

where c is the artificial sound speed. p_0 is usually chosen to achieve a small compressibility for the water phase, that is, $c_w \geq 10U_w^{\max}$ where $U_w^{\max}$ is the expected maximum velocity of water. After determining c_w and p_0, the sound speed of the air c_a can be determined by Equation (7).

2.3. Boundary conditions

In this study, the dummy particle method proposed by Adami *et al.* (2012) is used for boundary treatment, which ensures full support of the kernel interpolation. Specifically, in this method, several layers of particles are set as boundary particles at the initial moment and kept stationary throughout the simulation process. The pressure of each dummy particle can be calculated from the surrounding fluid particles, and their density can be obtained using the equation of state (i.e., Equation (5) or Equation (6)). To avoid non-physical phenomena such as boundary and particle adhesion, when calculating the density of the dummy boundary particles, the density is limited to not less than the initial density of the particles.

3. METHOD VALIDATION

The SPH simulation method used in this study is applied to two validation cases with single-phase and two-phase flows to demonstrate its performance. The first one is a dynamic water tank movement problem with theoretical solution, and the second is a typical dam break simulation whose results are known from the literature. In the parameter determination of resolution and artificial viscosity in these two cases, the parameter setting of $\Delta x = 0.01$ and $\alpha = 0.2$ in the dimensionless simulation of a 2D dam break by Adami *et al.* (2012) is used as a reference. A number of values between 10 and 20 times the maximum velocity as the artificial sound speed have been tried to determine the optimal value of the sound speed. To compare with the literature or theory, the results of both cases are expressed in the dimensionless form.

3.1. Case 1: water tank movement

In the dynamic water tank movement problem, a tank containing a homogeneous fluid moves horizontally to the right with a constant acceleration a. In this validation case, we set up a water tank with a length of 1 and a height of 1.5, and a water depth in the tank of 0.5 in dimensionless units. In the single-phase flow, the rest of the tank is vacuum, while in the two-phase flow, the rest is set to air with a density one-thousandth of that of water. In this case, it is assumed that the gravity is g and the acceleration $a = 0.5\,g$. The resolution and artificial viscosity used are $\Delta x = 0.01$ and $\alpha = 0.2$, which have been verified to be reliable according to Adami *et al.* (2012). Therefore, there are 5,000 and 15,000 fluid particles in the single-phase flow and two-phase flow simulations, respectively. The sound speed in the water phase is determined to be $c_w = 20U_w^{\max}$ based on the maximum water velocity, and then that in the air phase is determined using Equation (7). From the steady state results of the simulations shown in Figure 1, where x and y represent the length and height of the water tank, respectively, it can be calculated that the tangent of the free surface inclination angle θ is kept at 0.5 (i.e., $\tan\theta = 0.5$) from Figure 1(a), and the

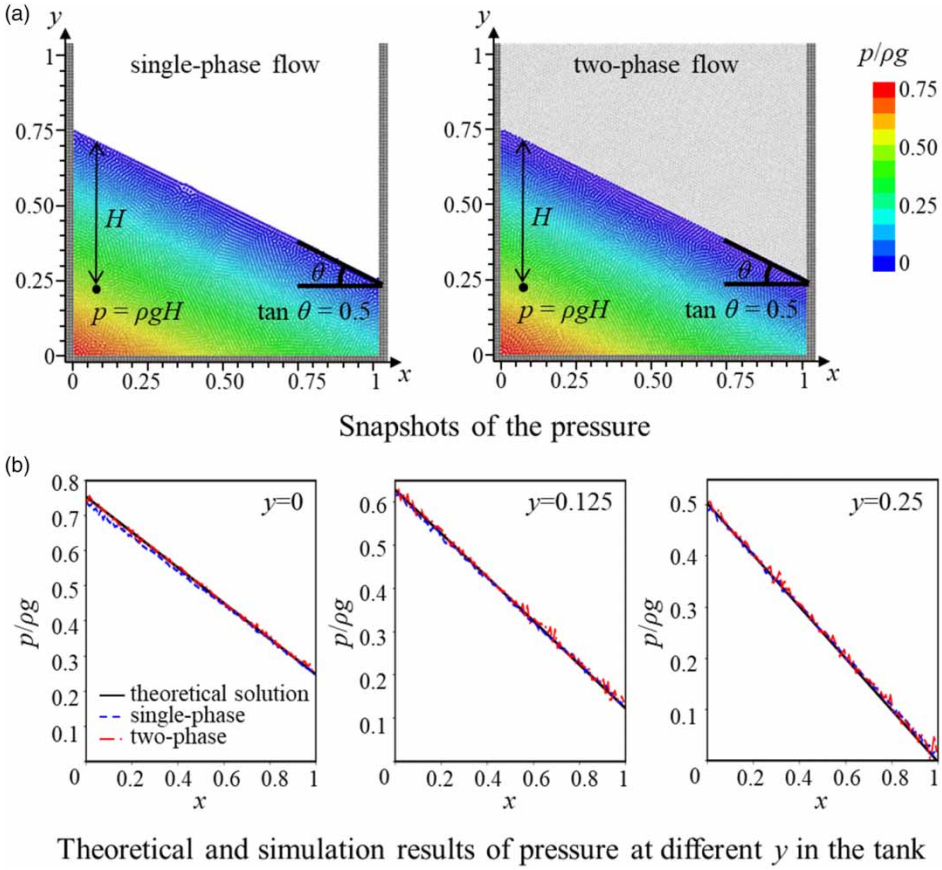

Figure 1 | Simulation results of water tank movement case.

pressure at any point inside the fluid is always related to the water depth (e.g., the pressure at the bottom of the leftmost side of the tank is $p = 0.75\rho g$ as shown in Figure 1(b)). According to the theoretical solution, the tangent of the surface angle and the pressure on the fluid are equal to a/g and ρgH, respectively. Therefore, the result obtained by the proposed method is consistent with the theoretical solution, indicating the reliability of the SPH simulation.

3.2. Case 2: dam break

In this case, the simulation domain is set to have a length of 5.366 and a height of 3. The water phase is a rectangle of size $L = 2$ and $H = 1$ initially covering the lower left side of the domain. As in Case 1, vacuum and air are taken in single-phase flow and two-phase flow, respectively. Following Adami *et al.* (2012), the resolution and the artificial viscosity parameters used in this case are $\Delta x = 0.01$ and $\alpha = 0.2$. Thus, a total of 20,000 and 140,980 fluid particles are used for single-phase and two-phase flow, respectively. After the dam is removed at the beginning, the water phase is dumped and the flow develops along the bottom due to gravity, impacting against the downstream vertical wall.

In Figure 2(a), the images of single-phase and two-phase flow of the dam break simulation are presented, where the color of the particles shows the local non-dimensional pressure between $p = 0$ (blue color) and $p = 1$ (red color). These images reveal that the main features of the evolution of the water phase flow are similar in single-phase and two-phase simulations. That is, the water initially travels along the bottom and is deflected sharply upward after hitting the wall. Then, due to gravity, the speed of the upward motion is reduced, and the flow flips back to the bottom, creating a cavity. In addition, it is also observed that the movement of water is more hindered in the presence of air, for example, the height of rise of the peak of two-phase flow at $t(g/H)^{1/2} = 7.4$ is lower than that of single-phase flow. These results are consistent with the simulation results of Adami *et al.* (2012), which indicate that the SPH method used in this study can accurately reflect the process of dam break.

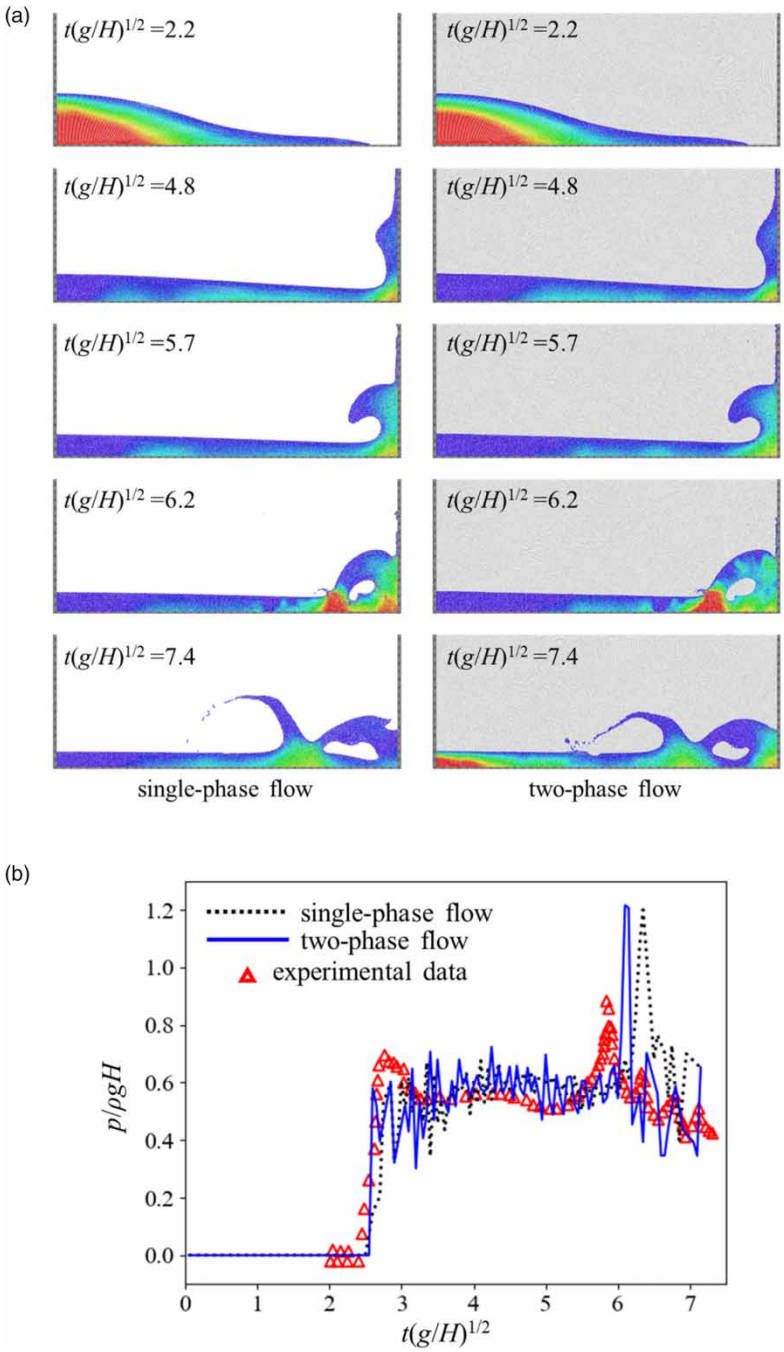

Figure 2 | Simulation results of dam break case. (a) Images of the pressure at each time of single-phase and two-phase dam break simulation. (b) Comparison of temporal pressure profile at $y/H = 0.2$ between SPH simulation and experimental data (Buchner 2002).

For a quantitative validation, the temporal pressure profile on the downstream wall is used as a comparison index. Figure 2(b) shows the result of the pressure on the downstream wall at $y/H = 0.2$ over time obtained by our simulation and the experimental data measured by Buchner (2002). As expected, the pressure distribution obtained by our SPH simulations is quite well captured. It can be seen from this figure that both the single-phase flow and the two-phase flow have two peaks, which are, respectively, caused by the impact of the water on the vertical wall and the formation of the cavity. Interestingly, the second peak in the two-phase flow comes before that in single-phase flow, which is closer to the experimental data. This is because in the two-phase flow, the air is trapped in the cavity, creating an air cushion effect and an immediate

increase in pressure. In contrast, in the single-phase flow, there is no air cushion effect and the pressure does not rise until it is impacted by the crushing pressure of the cavity. The results demonstrate that the two-phase simulation can capture more details so that it reflects the realistic situation better and has higher reliability than the single-phase simulation.

4. PIPE FLOW APPLICATION

4.1. Case description

A dimensionless model constructed in this study is shown in Figure 3, including specific parameters and their values. The model consists of an upstream tank, a downstream tank, and a pipe, representing the upstream and downstream manholes as well as the stormwater pipe in the real rainwater drainage system. In this model, the length and height of the two tanks are both set to 1 (i.e., $B_U = H_U = B_D = H_D = 1$), the distance between these two tanks is $L = 2$, and they are connected by the pipe. The center of the pipe is 0.4 above the bottom of the upstream tank, and the diameter and slope of the pipe are i and D, respectively. At the start of the simulation, the upstream tank has an initial water level H, while the downstream one has no water. The water at the upstream tank flows into the downstream one through the pipe, simulating the drainage process of free flow with non-jacking downstream of the pipe in reality.

In this study, there are two setting modes for the areas where there is no water in the two tanks and the pipe, which are set to vacuum (i.e., no particles are placed) and set to air (i.e., filled with air particles) to explore the impacts of air on the pipe flow state development. The simulation follows the dimensionless model, where the characteristic length is the height of the upstream tank H_U, the density of water is $\rho_w = 1$, and the gravity is $g = -1$ along the z direction. We shall explore the influence of air on the pipe flow under different upstream water levels, pipe diameters, and pipe slopes, which are summarized in Table 1. It should be noted that the selection of the slope parameters refers to the actual engineering values, which are the design values commonly used in practice.

4.2. Convergence study

A convergence study is carried out on the particle resolution, which affects the accuracy of the numerical simulations. In Figure 4, we show the SPH simulation results of single-phase flow and two-phase flow at different resolutions under the scenario $H = 0.7$, $D = 0.14$, and $i = 1\%$. The three resolutions used in Figure 4 are $\Delta x = 0.01$, 0.005, and 0.0025, and according to Adami *et al.* (2012) and Equation (4), the coefficient α at different resolutions is 0.2, 0.4, and 0.8, respectively. The sound speed of water is set to $c_w = 10U_w^{\max}$ to make sure the rate of change of the particle density is kept within 1%. It can be

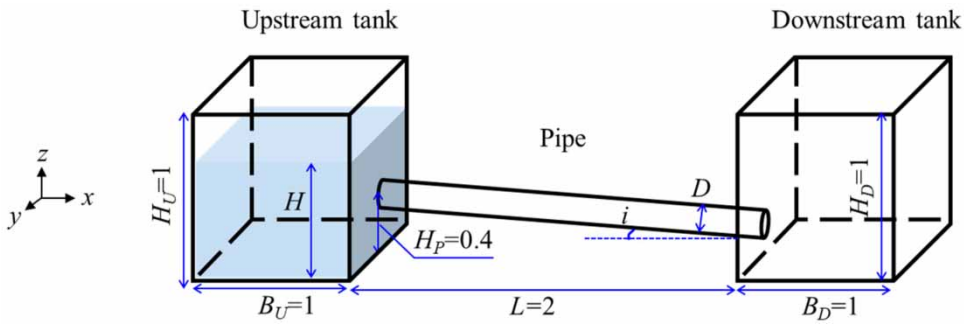

Figure 3 | Sketch of the numerical model with relevant parameters and their values.

Table 1 | Model variables

Variable name and definition	Range of values
H: Upstream water level	0.5, 0.7, and 0.9
D: Pipe diameter	0.1, 0.14, and 0.18
i: Pipe slope	0.5, 1, and 2%

seen from Figure 4(a) that the single-phase flow simulation results of these three resolutions are highly consistent. However, there are some differences in the two-phase flow simulation results. Specifically, in the two-phase flow simulation, compared to the resolutions of $\Delta x = 0.005$ and 0.0025, the full flow appears earlier in the resolution of $\Delta x = 0.01$, and its distance is much longer; see the images at $t(g/H)^{1/2} = 2$ and $t(g/H)^{1/2} = 3$ in Figure 4(b). This is because the particles are too large at low resolution to accurately characterize the water and air near the pipe walls. While the simulation results of $\Delta x = 0.005$ and 0.0025 are similar, considering the computational cost, $\Delta x = 0.005$ is applied as the resolution for the SPH simulations in this study.

4.3. Comparison of 2D and 3D simulation results

We also compare the results of the two-dimensional (2D) simulation and the three-dimensional (3D) simulation. The length of the third direction of the 3D simulation is 1, and the value of α is determined according to Equation (4). Taking the scenarios $H = 0.7$, $D = 0.1$, and $i = 1\%$ as an example, the result is shown in Figure 5. Note that 2D modeling is the field of a median longitudinal section of the circle pipe; the results only represent the computational field of a median longitudinal section since the transverse section of the pipe is not rectangular in shape. For comparison, the simulation results of the median longitudinal section of the pipe in 3D modeling are shown in Figure 5. The images in Figure 5(a) indicate that 2D and 3D simulations give highly consistent results for both single-phase and two-phase simulations. Furthermore, it can be seen

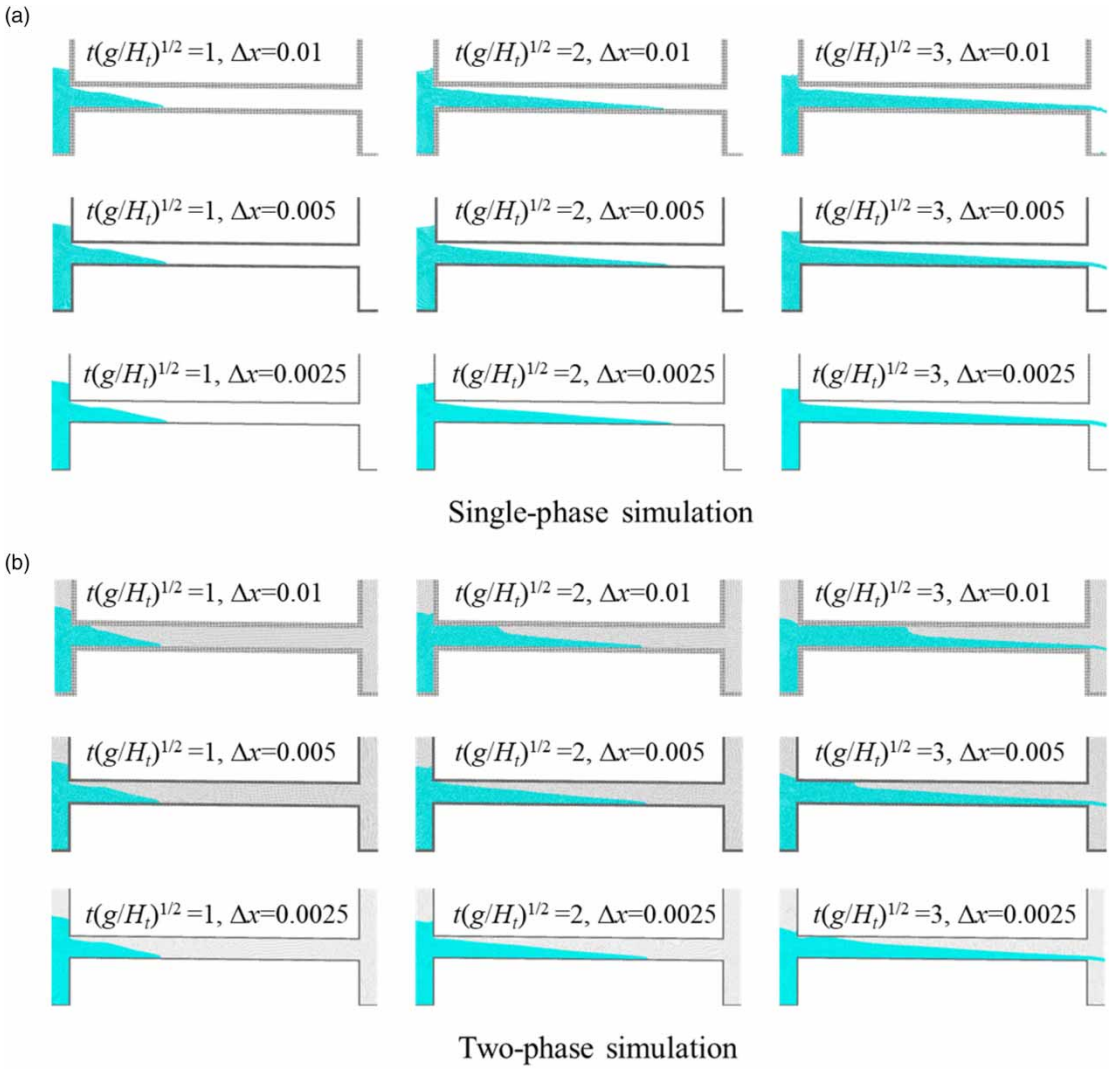

Figure 4 | Images of the simulation for three different resolutions when $H = 0.7$, $D = 0.14$, and $i = 1\%$.

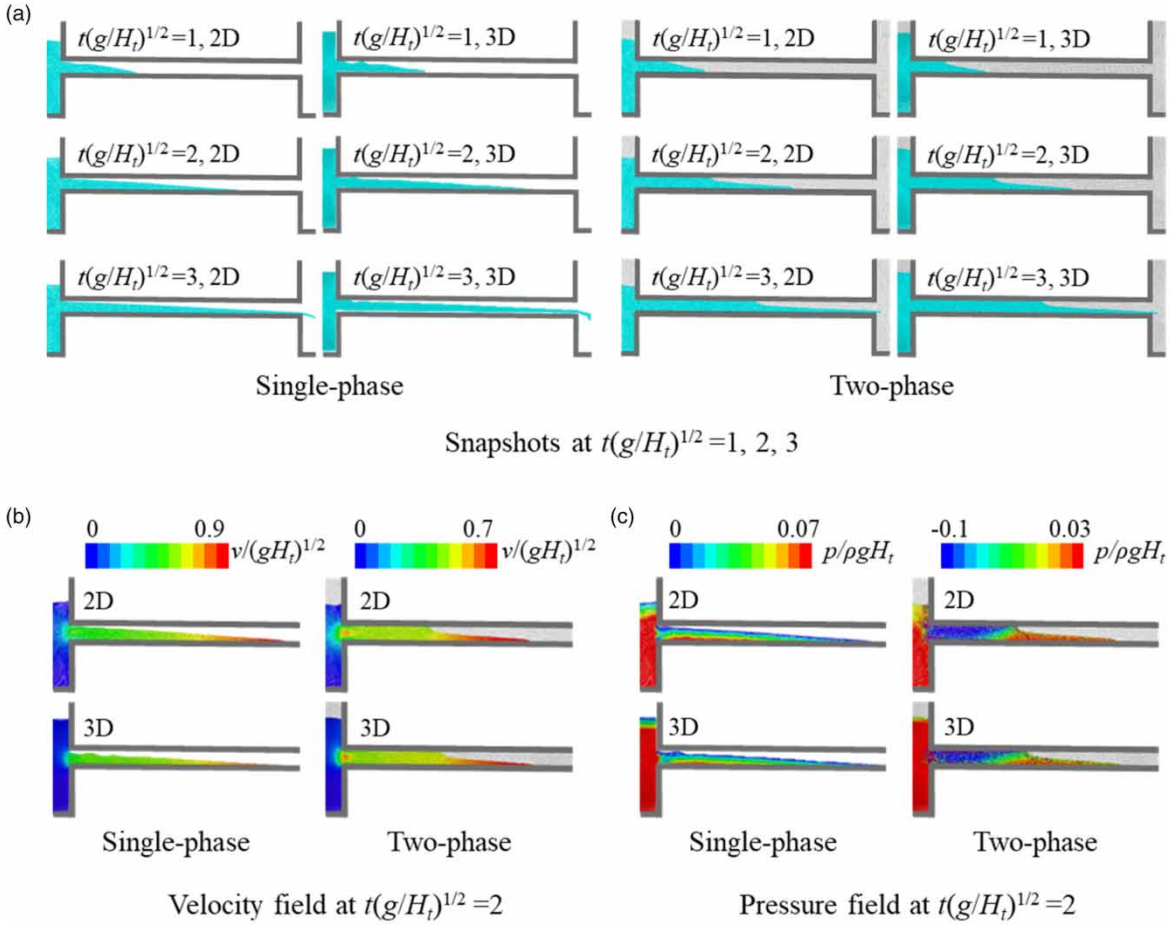

Figure 5 | Comparison of 2D and 3D simulation results when $H = 0.7$, $D = 0.1$, and $i = 1\%$.

from Figure 5(b) and 5(c) that the velocity field and pressure field between the 2D and 3D simulations are also similar. The pipe flow state and development process obtained by the 2D simulation are the same as those obtained by the 3D simulation. Therefore, considering the computational cost, 2D simulations are mainly considered in the following study in this paper, which is acceptable as the median longitudinal section of the pipe is a representative cross-section of the pipe flow.

4.4. Results and discussion

4.4.1. Pipe flow rates versus upstream water levels

The numerical method is first applied to three cases with different H to investigate the relationship between upstream water levels and the impacts of air on pipe flow states development. In this section, the diameter and slope of the pipe are irrelevant variables, which are set to 0.1 and 1% universally for each case. The comparison results of the flow rates in vacuum state (i.e., single-phase flow) and air state (i.e., two-phase flow) at different upstream water levels are shown in Figure 6(a)–6(c), and the flow rate differences between single-phase flow and two-phase flow are shown in Figure 6(d).

It can be seen from Figure 6(a) that when $H = 0.5$, the influence of air can be ignored, as the evolutions of the flow rate for single-phase and two-phase flows are the same. However, in the case of $H = 0.7$ and 0.9 (see Figure 6(b) and 6(c)), the presence of air has a significant impact on the pipe flow rate. To be specific, in the presence of air, the pipe flow rate is first higher than that in vacuum and remains so for some time (approximately $t(g/H)^{1/2} = 6.2$ for $H = 0.7$ and $t(g/H)^{1/2} = 6.6$ for $H = 0.9$). Subsequently, the flow rate in the presence of air decreases below that of the vacuum. The decrease in the flow rate of the two-phase flow in the later stage of drainage is expected because the amount of water in the upstream water tank is constant, and the two-phase flow discharges more water than the single-phase flow in the early stage. Therefore, we shall mainly explore the reasons why the flow rate of the two-phase flow is higher than that of single-phase flow in the early stage.

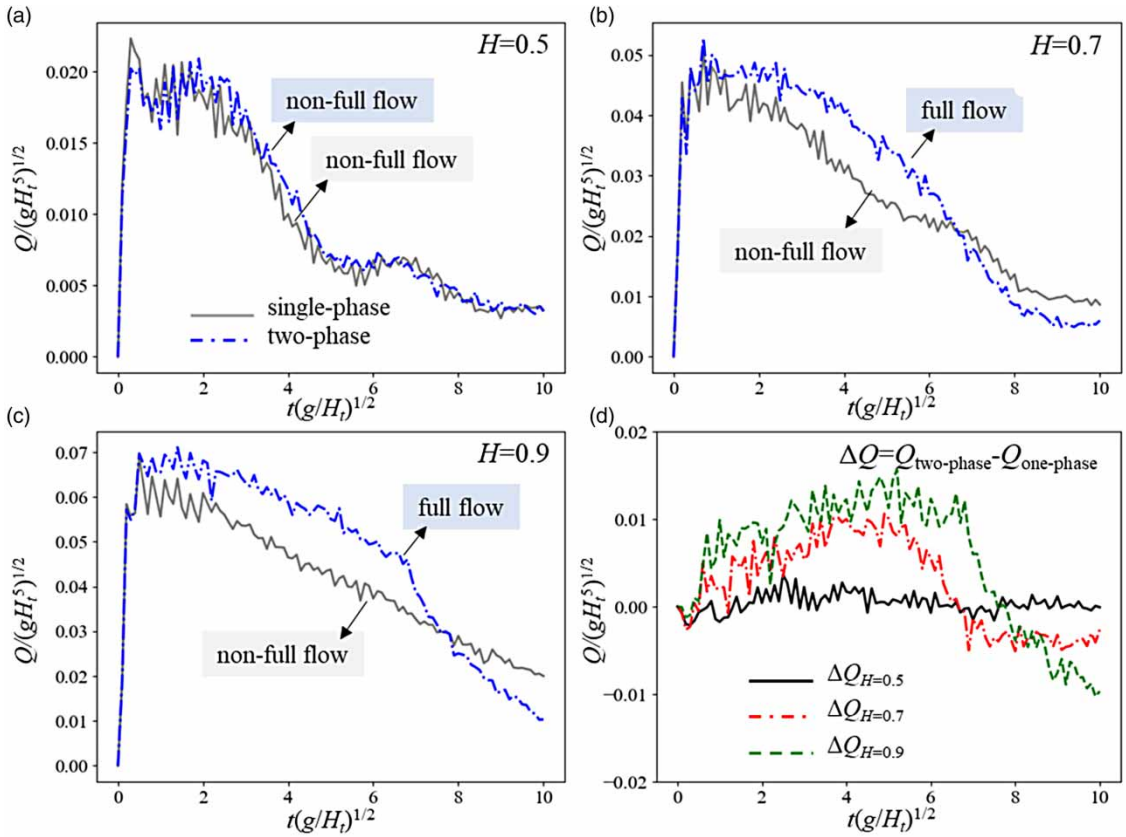

Figure 6 | Pipe flow rate of single-phase flow and two-phase flow during the drainage process under different upstream water levels $H = 0.5$, 0.7, and 0.9.

Figure 7 shows the images of the single-phase flow and two-phase flow simulation results of each case at $t(g/H)^{1/2} = 1$, 3, and 5. It can be seen from Figure 7(a) that in the case of $H = 0.5$, whether air is present or not, the pipe is in a non-full flow state, whereas in the cases of $H = 0.7$ and 0.9, as shown in Figure 7(b) and 7(c), the pipe presents non-full flow in the single-phase simulation but full flow in the two-phase simulation. These comparison results indicate that only when there are differences in the flow states of single-phase and two-phase flows, there is a large difference in their flow rates. Since the flow areas (shown as water depths in this figure) at the entrance of the pipe are the same for both single-phase flow and two-phase flow for each case at different times, the difference in the flow rate for $H = 0.7$ and 0.9 is mainly caused by the difference in flow velocity.

Furthermore, note the distance between the upstream water levels on the left and the top of the pipe in Figure 7; it can be seen that under full flow conditions, the upstream water level is higher than the top of the pipe. This reflects a necessary condition for the formation of full flow in two-phase flow, that is, *the upstream water level must be higher than the top of the pipe to prevent air from being discharged from the upstream end*.

To further explore the impact of air at different upstream water levels on the pipe flow state development and flow rate, taking $H = 0.5$ and 0.9 as examples, the flow velocity and pressure distributions at the entrances of pipe under these two cases at time $t(g/H)^{1/2} = 4$ are plotted in Figure 8. It can be seen from Figure 8(a) that in the case of $H = 0.5$, in the two-phase flow with air, the flow state and velocity field distribution are consistent with the vacuum state, while in the case of $H = 0.9$ shown in Figure 8(b), in the two-phase simulation, the flow state is full flow and the inlet flow velocity (up to about 0.8) is significantly higher than that in the vacuum state (about 0.6). If we inspect the pressure field at this location, as shown in Figure 8(d), in the full flow state of the two-phase flow (i.e., in the presence of air), a large negative pressure area appears in the pipe, and a siphon-like phenomenon occurs (Potter & Barnes 1971). This creates a suction effect, which accelerates the flow velocity of the water at the entrance of the pipe. While in the single-phase flow (i.e., vacuum state), there is no negative pressure in the pipe, so the water flows only under the action of gravity, which gives it a lower

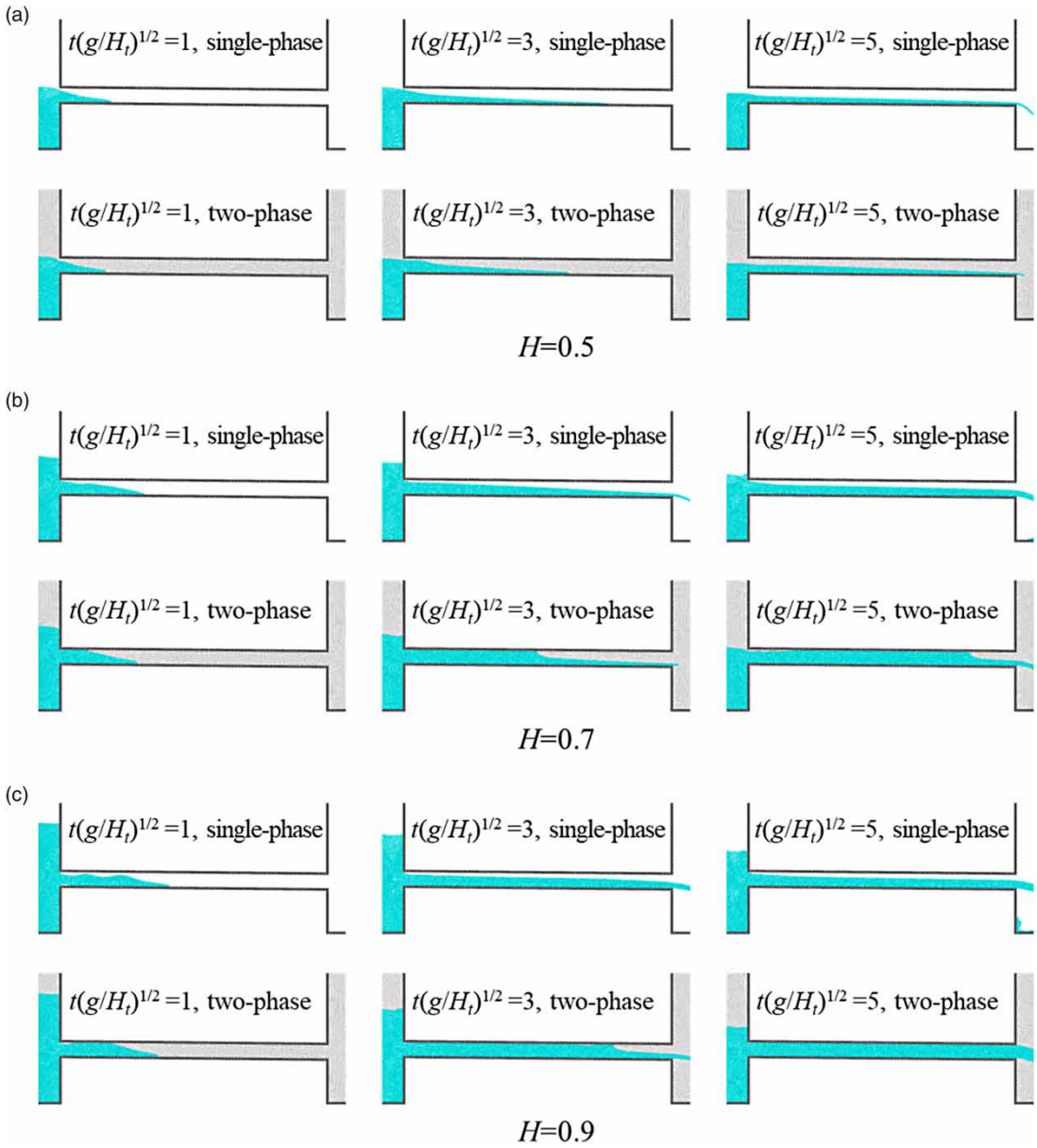

Figure 7 | Snapshots of the pipe flow states for single-phase flow and two-phase flow at $t(g/H)^{1/2} = 1$, 3, and 5 under different upstream water levels.

velocity. If the two-phase flow does not form a full flow state, for example, in the case of $H = 0.5$ (shown in Figure 8(c)), no siphon will form, resulting in the same pressure and flow velocity distribution as in vacuum.

4.4.2. Pipe flow rates versus pipe diameters

This section focuses on the influence of air on the pipe flow state development and flow rate under different pipe diameters. A case with $H = 0.7$ and $i = 1\%$ is used for comparative analysis. Figure 9 presents the flow rate results of the vacuum (i.e., single-phase flow) and air (i.e., two-phase flow) conditions of different pipe diameters. Comparison of the results in Figure 9(a-c) reveals that as the pipe diameter D increases, the influence of air on the flow rate gradually decreases, which is reflected in the fact that the curves of single-phase and two-phase flow gradually approach each other, and the difference becomes smaller (shown in Figure 9(d)). When the pipe diameter D increases to 0.18, the pipe flow rate with or without air is almost the same (see Figure 9(c)).

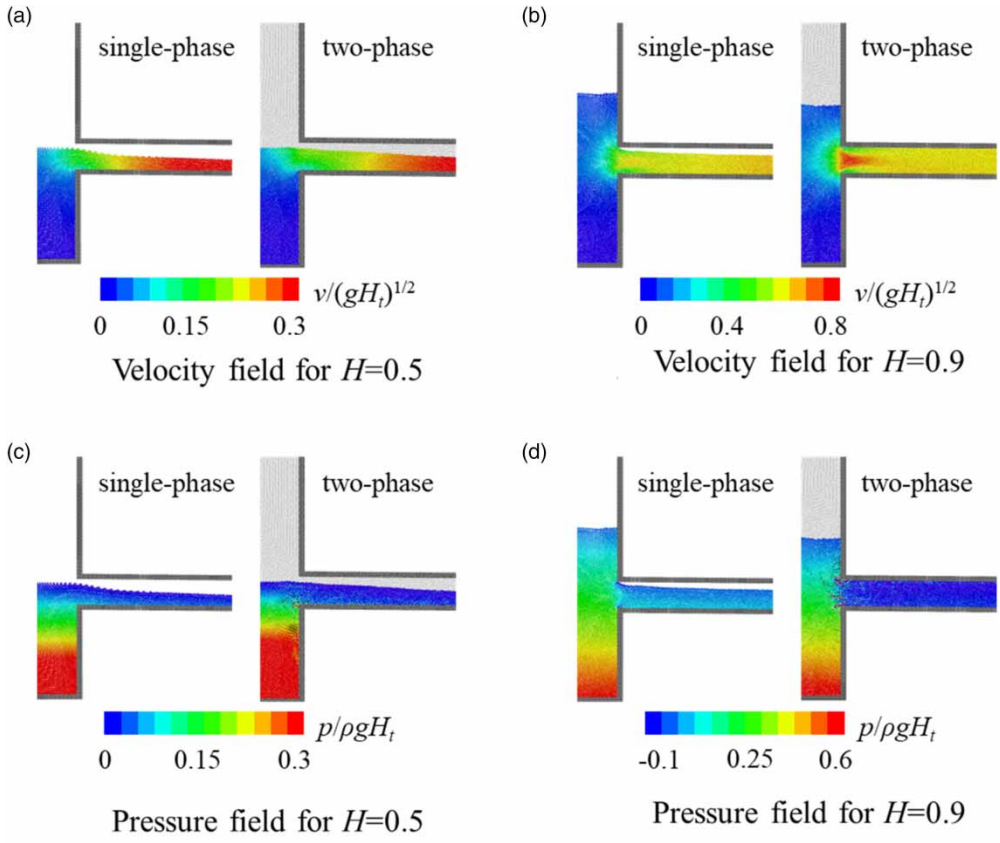

Figure 8 | Flow velocity and pressure fields in the entrance of pipe at $t(g/H)^{1/2} = 4$ under $H = 0.5$ and 0.9.

The pipe flow state for single-phase and two-phase flow of each case at three times $t(g/H)^{1/2} = 1$, 2, and 3 are shown in Figure 10, which denotes that the reason for the flow rate difference is still related to the flow pattern of the pipe. Specifically, when $D = 0.1$ (see Figure 10(a)), full flow is formed in the presence of air, so the difference between the two is large, and the difference arises at the initial moment. When $D = 0.14$, as shown in Figure 10(b), the full flow state occurs at a certain time between $t(g/H)^{1/2} = 2$ and 3. Correspondingly, the flow rate curves of the single-phase and two-phase flow remain consistent before $t(g/H)^{1/2} = 2$ and begin to differ at a certain point later (i.e., when full flow is formed). When the pipe diameter D increases to 0.18, the pipe is in a non-full flow state regardless of the presence of air (Figure 10(c)), and the difference in flow rate is negligible (see Figure 9(c)).

Moreover, the upstream water level used in this case is 0.7, which is higher than the top of the pipe, but there is still a situation of non-full pipe flow, such as $D = 0.18$ (see Figure 10(c)). This is because, in the two-phase flow, the water flow in the pipe is blocked by air, and the water level will rise for a certain distance (Chanson 2009). *Only when the water level reaches the top of the pipe due to air resistance can full flow be formed.* Larger pipe diameters usually require a higher rising water level, which is difficult to achieve. Therefore, an increase in the pipe diameter may result in a non-full flow state.

4.4.3. Pipe flow rates versus pipe slopes

We set the upstream water level to $H = 0.7$, and select pipes with diameter $D = 0.1$ and different slopes (i.e., $i = 0.5$, 1, and 2%, commonly used slopes for drainage pipes in real engineering) for the simulation to study the impact of air on the pipe flow under different pipe slopes. The results show that in this condition (i.e., $H = 0.7$ and $D = 0.1$), the influence of air on pipe flow under different slopes is very consistent. To be specific, for the three different slopes, the results for single-phase flow are the same and so are those for two-phase flow; the flow curves of single-phase flow and two-phase flow are consistent

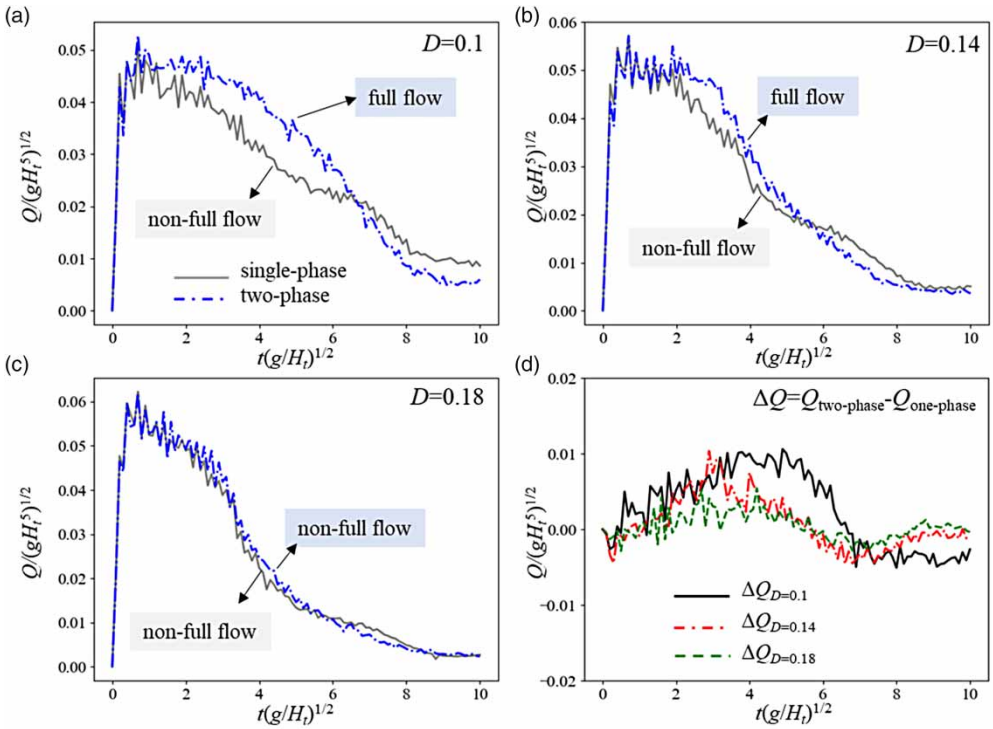

Figure 9 | Pipe flow rate of single-phase flow and two-phase flow during the drainage process under different pipe diameters $D = 0.1$, 0.14, and 0.18.

with Figure 6(b). This indicates that the presence of air has a significant impact on the flow rate for these three slopes, and the flow states of single-phase and two-phase flows are similar to Figure 7(b). Similar to Sections 4.4.1 and 4.4.2, this phenomenon of different pipe flow state and flow rate is caused by the difference of flow state in vacuum and in air. That is, the pipe flow rate difference is the result of the velocity difference caused by non-full flow in vacuum state and full flow in air state. In addition, the results can also show that the slope commonly used in practice has little impact on the air–water state in the pipe.

In the free flow situation with non-jacking downstream considered in this study, the presence of air can contribute to the formation of a full flow in the pipe under certain circumstances, as compared to a vacuum. When a full flow is formed in the pipe, the siphon-like phenomenon is created at the pipe inlet and the discharge volume of the pipe is increased. The results in this section indicate that the presence of air in a pipe can affect the development of the pipe flow state and the pipe flow rate, despite the fact that the air is not trapped. In contrast to the commonly recognized blocking effect of trapped air in submerged flow, air in free flow is able to promote pipe draining. This finding refines the understanding of air–water flow in pipes and is of practical importance.

5. SUMMARY AND CONCLUSION

In this study, the impacts of air on pipe flow state development and flow capacity were explored by SPH simulations. The numerical SPH method was first validated by two cases with a theoretical solution or with known results from the literature and then applied to the pipe flow simulations. Single-phase flow (i.e., no air) and two-phase flow (i.e., air and water) in pipes were simulated to analyze the impacts of air in the case of non-jacking downstream of the pipes. The main findings and implications of this study are summarized as follows:

(1) Compared with commonly used grid methods, the SPH method used in this study has outstanding advantages in capturing the free surface and air–water interface. This method accurately simulates both vacuum and air states in the pipe and helps in clearly studying the underlying hydraulic interactions between air and pipe flow state development.

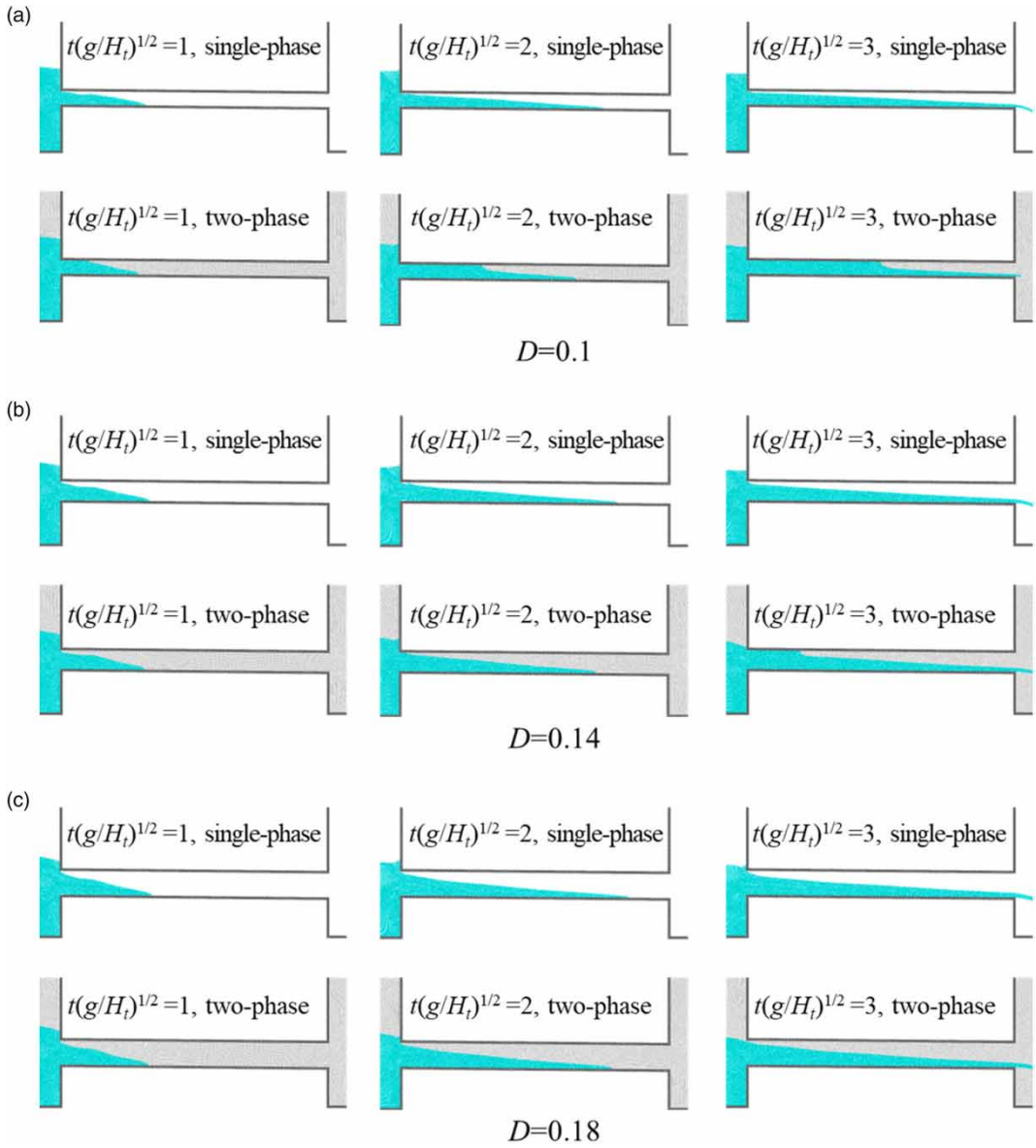

Figure 10 | Snapshots of the pipe flow states for single-phase flow and two-phase flow at $t(g/H)^{1/2} = 1$, 2, and 3 under different pipe diameters.

(2) In the single-phase flow, the pipe flow state is always a non-full flow state. It is only when air is present that a full flow state may be observed in the pipe. There are two necessary conditions for the formation of full pipe flow in the presence of air. One necessary condition is that the upstream water level is higher than the top of the pipe entrance, so air cannot escape from the upstream end. And the other one is the height at which the water level rises in the pipe when affected by air resistance must reach the top of the pipe.

(3) The presence of air will affect the flow state and flow rate in the pipe. When the pipe forms a full flow in the two-phase flow, a negative pressure appears in the pipe, causing a siphon-like effect. The flow velocity at the entrance of the pipe will increase because of the siphon-like phenomenon, resulting in an increase in the flow rate. The earlier the full flow occurs and the longer the length, the more obvious the increase in flow rate will be. Compared to the single-phase flow, the presence of air promotes the flow capacity of the pipe when full flow occurs.

We believe that the numerical results of this study can improve the understanding of the complex interacting processes between air and pipe flow state development. The findings of this study can be of importance to engineering applications

for stormwater pipe design and urban flood prevention. It is acknowledged that a limitation of this study may exist, that is, the 2D modeling only focuses on the median longitudinal section of the circle pipe and does not provide a complete picture of the pipe flow in each cross-section of a circular pipe. In future studies, 3D modeling can be conducted to learn more details about individual cross-sections, which may lead to more comprehensive and complete information and perceptions of the air impacts on the state development of pipe flow.

ACKNOWLEDGEMENTS

This study was supported by the National Key R&D Program of China (Grant No. 2022YFC3200032). XB received the starting grant from 100 Talents Program of Zhejiang University. Furthermore, FZ would like to appreciate the support from the National Natural Science Foundation (NSFC) of China (Grant Nos.: 52261160379 and 52179080).

DATA AVAILABILITY STATEMENT

Data cannot be made publicly available; readers should contact the corresponding author for details.

CONFLICT OF INTEREST

The authors declare there is no conflict.

REFERENCES

Adami, S., Hu, X. Y. & Adams, N. A. 2012 A generalized wall boundary condition for smoothed particle hydrodynamics. *Journal of Computational Physics* **231** (21), 7057–7075.

Buchner, B. 2002 *Green Water on Ship Type Offshore Structures*. PhD. Thesis, Technische Universiteit Delft, Delft.

Cai, X., Li, Z. & Bian, X. 2023 Arbitrary slip length for fluid-solid interface of arbitrary geometry in smoothed particle dynamics. *Journal of Computational Physics* **494**, 112509.

Chanson, H. 2009 Application of the method of characteristics to the dam break wave problem. *Journal of Hydraulic Research* **47** (1), 41–49.

ChinaNews 2022 *Investigation Report on '7·20' Heavy Rainstorm Disaster in Zhengzhou, Henan Released*. Available from: http://www.chinanews.com.cn/gn/2022/01-21/9658591.shtml.

Dong, X., Hao, G. & Yu, R. 2022 Two-dimensional smoothed particle hydrodynamics (SPH) simulation of multiphase melting flows and associated interface behavior. *Engineering Applications of Computational Fluid Mechanics* **16** (1), 588–629.

He, J., Hou, Q., Lian, J., Tijsseling, A. S., Bozkus, Z., Laanearu, J. & Lin, L. 2022 Three-dimensional CFD analysis of liquid slug acceleration and impact in a voided pipeline with end orifice. *Engineering Applications of Computational Fluid Mechanics* **16** (1), 1444–1463.

Hou, Q., Zhang, L. X., Tijsseling, A. S. & Kruisbrink, A. C. H. 2012 Rapid filling of pipelines with the SPH particle method. *Procedia Engineering* **31**, 38–43.

Hu, X. Y. & Adams, N. A. 2006 A multi-phase SPH method for macroscopic and mesoscopic flows. *Journal of Computational Physics* **213** (2), 844–861.

Lind, S. J., Stansby, P. K., Rogers, B. D. & Lloyd, P. M. 2015 Numerical predictions of water–air wave slam using incompressible–compressible smoothed particle hydrodynamics. *Applied Ocean Research* **49**, 57–71.

Liu, G. R. & Liu, M. B. 2003 Smoothed particle hydrodynamics: A meshfree particle method. World Scientific, Singapore. p. 13–14.

Meister, M. & Rauch, W. 2015 Modelling aerated flows with smoothed particle hydrodynamics. *Journal of Hydroinformatics* **17** (4), 493–504.

Meng, Z. F., Ming, F. R., Wang, P. P. & Zhang, A. 2021 Numerical simulation of water entry problems considering air effect using a multiphase Riemann-SPH model. *Advances in Aerodynamics* **3** (1), 1–16.

Monaghan, J. J. 1994 Simulating free surface flows with SPH. *Journal of Computational Physics* **110** (2), 399–406.

Potter, A. & Barnes, F. H. 1971 The siphon. *Physics Education* **6** (5), 362.

Pozos, O., Gonzalez, C. A., Giesecke, J., Marx, W. & Rodal, E. A. 2010 Air entrapped in gravity pipeline systems. *Journal of Hydraulic Research* **48** (3), 338–347.

Qian, Y., Shao, W., Zhu, D. Z., Mohamad, K. A., Steffler, P. M., Edwini-Bonsu, S., Yue, D. & Krywiak, D. 2021 Modeling air flow in sanitary sewer systems: A review. *Journal of Hydro-Environment Research* **38**, 84–95.

Song, W., Yan, H., Li, F., Tao, T., Duan, H., Xin, K. & Li, S. 2023 Development of smoothed particle hydrodynamics based water hammer model for water distribution systems. *Engineering Applications of Computational Fluid Mechanics* **17** (1), 2171139.

Vasconcelos, J. & Wright, S. J. 2007 Experimental investigation on surcharging of flowing sewers. *Journal of Water Management Modeling* **10**, 210–219.

Wang, Y. C., Nobi, N., Nguyen, T. & Vorreiter, L. 2012 A dynamic ventilation model for gravity sewer networks. *Water Science and Technology* **65** (1), 60–68.

Wang, K., Liang, H., Zhao, C. & Bian, X. 2023 Dynamics of a droplet in shear flow by smoothed particle hydrodynamics. *arXiv preprint arXiv*. 2307.02807.

Winsemius, H. C., Aerts, J. C., Van Beek, L. P., Bierkens, M. F., Bouwman, A., Jongman, B., Kwadijk, J. C. J., Ligtvoet, W., Lucas, P. L., van Vuuren, D. P. & Ward, P. J. 2016 Global drivers of future river flood risk. *Nature Climate Change* **6** (4), 381–385.

Zhang, A., Sun, P. & Ming, F. 2015 An SPH modeling of bubble rising and coalescing in three dimensions. *Computer Methods in Applied Mechanics and Engineering* **294**, 189–209.

Zheng, F., Westra, S. & Leonard, M. 2015 Opposing local precipitation extremes. *Nature Climate Change* **5** (5), 389–390.

Zhou, L., Liu, D. & Karney, B. 2013 Investigation of hydraulic transients of two entrapped air pockets in a water pipeline. *Journal of Hydraulic Engineering* **139** (9), 949–959.

First received 8 October 2023; accepted in revised form 25 January 2024. Available online 8 February 2024